Electronic Supplementary Material (ESI) for New Journal of Chemistry.
This journal is © The Royal Society of Chemistry and the Centre National de la Recherche Scientifique 2020

New Journal of Chemistry

Dramatic Luminescence Signal from a Co(II) based Metal Organic Compound due to Construction of Charge Transfer Bands with Al^{3+} and Fe^{3+} ions in Water: Steady Sate and Time Resolved Spectroscopic Studies

Pooja Daga,[a] Prakash Majee,[a] Debal Kanti Singha,[a,b] Priyanka Manna,[b] Sayani Hui,[b] Ananta Kumar Ghosh,[c] Partha Mahata[b*] and Sudip Kumar Mondal[a*]

[a]Department of Chemistry, Siksha-Bhavana, Visva-Bharati University, Santiniketan-731235, West Bengal, India. Email: sudip.mondal@visva-bharati.ac.in

[b]Department of Chemistry, Jadavpur University, Jadavpur, Kolkata-700 032, West Bengal, India.

Email: parthachem@gmail.com

[c]Department of Chemistry, Burdwan Raj College, Burdwan, Burdwan-713104, West Bengal, India

ELECTRONIC SUPPLEMENTARY INFORMATION

* Corresponding Authors, E-mail: sudip.mondal@visva-bharati.ac.in, parthachem@gmail.com

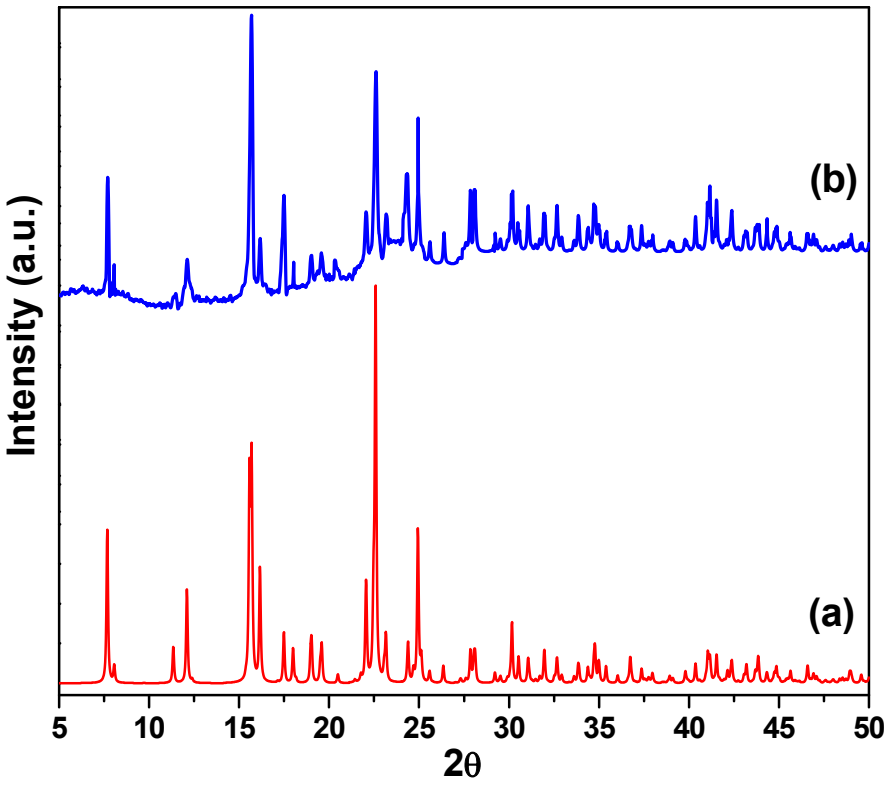

Fig. S1. Powder XRD (CuKα) patterns of [Co(bpds)(bdc)(H_2O)$_2$].bpds, **1**: (a) simulated from single crystal X-ray data, (b) experimental.

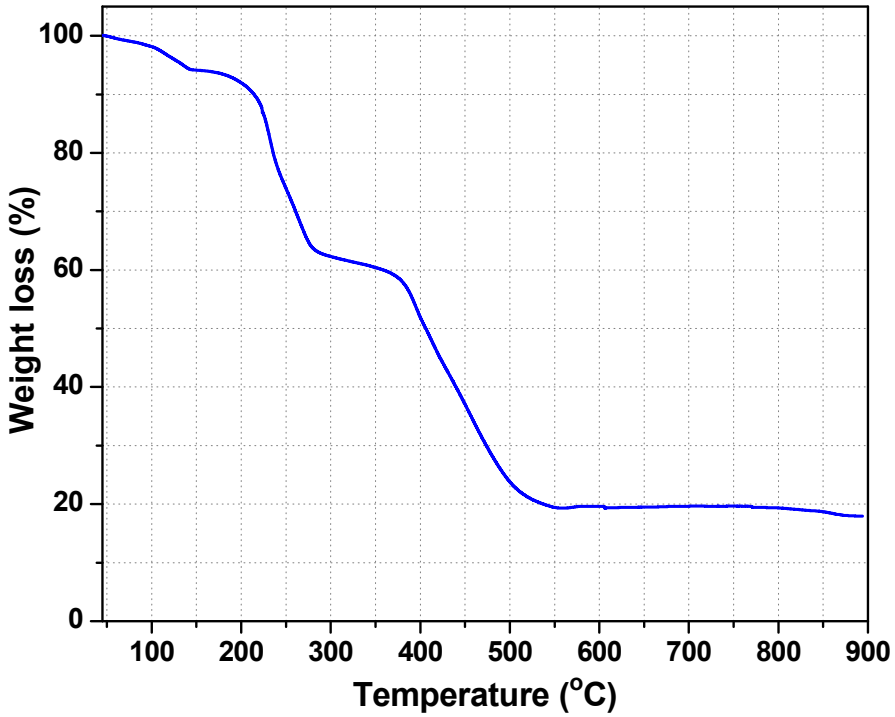

Fig. S2. Thermogravimetric analysis (TGA) data of [Co(bpds)(bdc)(H_2O)$_2$].bpds, **1**, in nitrogen atmosphere. The plot shows % weight loss of **1** with increase in temperature.

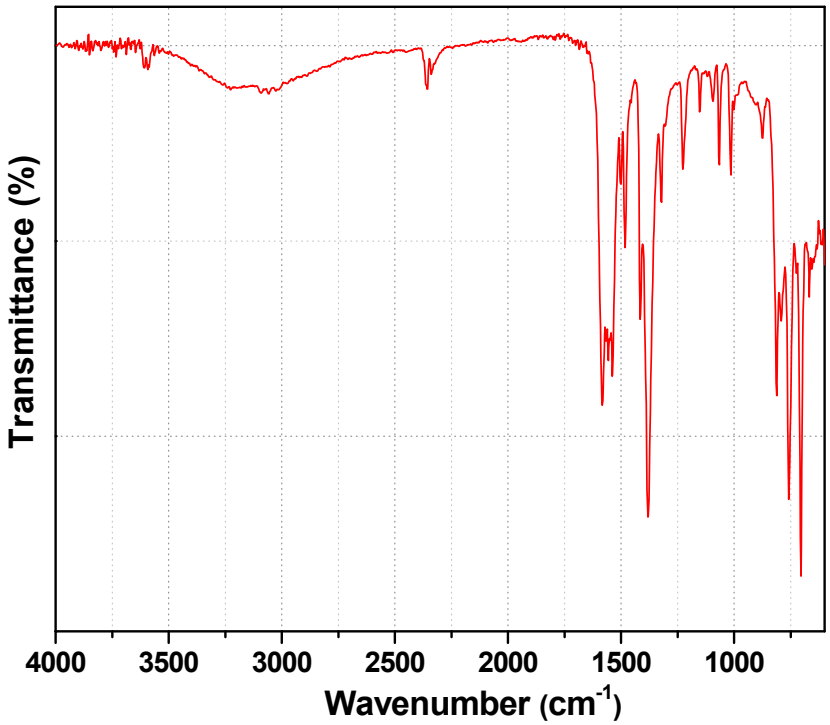

Fig. S3. IR spectrum of [Co(bpds)(bdc)(H_2O)$_2$].bpds, **1**.

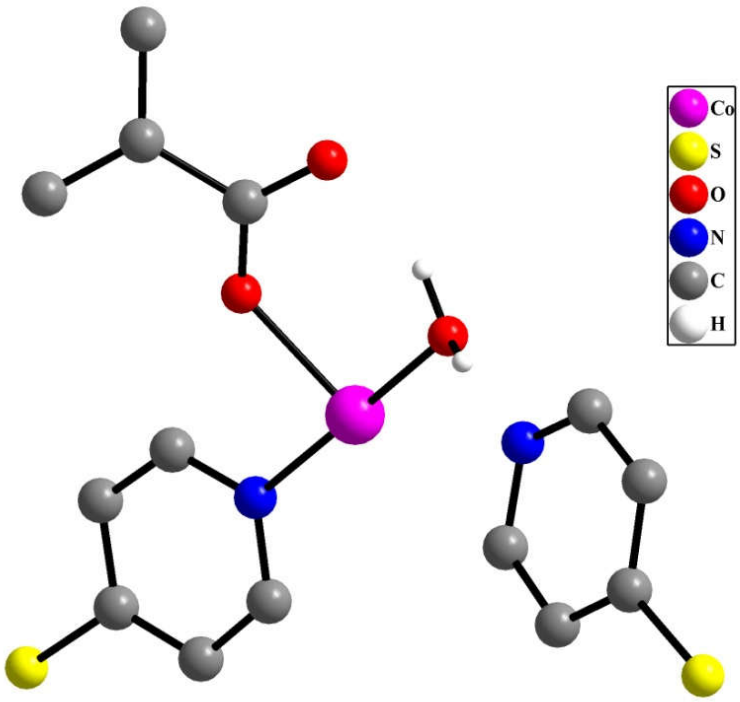

Fig. S4. Figure shows asymmetric unit in the structure of [Co(bpds)(bdc)(H_2O)$_2$].bpds, **1**.

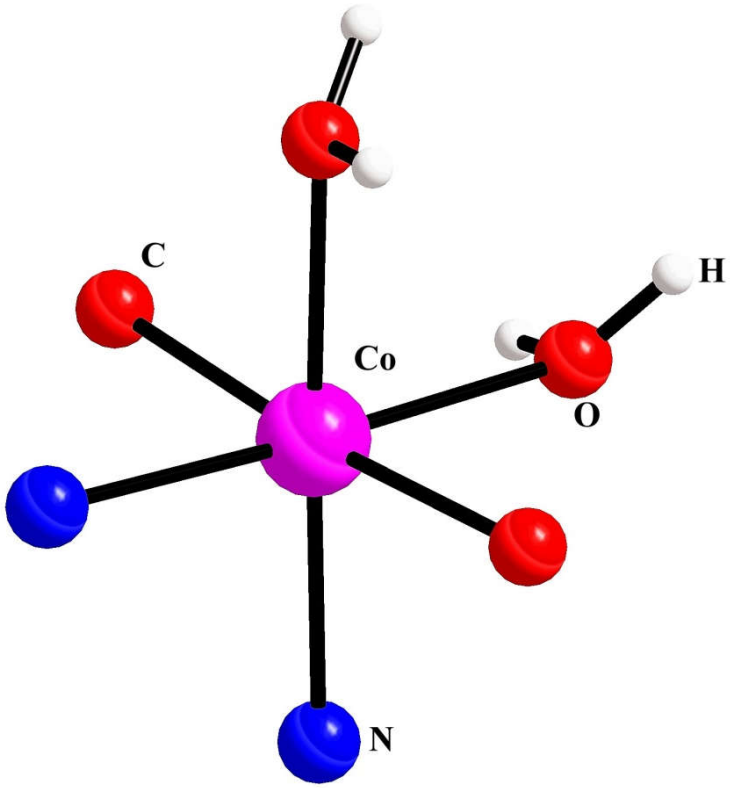

Fig. S5. Figure shows the octahedral coordination around Co^{2+} ion in $[Co(bpds)(bdc)(H_2O)_2].bpds$, **1**.

Table S1: Selected bond distances (Å) observed in [Co(bpds)(bdc)(H_2O)$_2$].bpds, **1**.

Bond	Distances, Å	Bond	Distances, Å
Co(01)-O(1)	2.0758(18)	Co(01)-O(3)#1	2.127(2)
Co(01)-O(1)#1	2.0759(19)	Co(01)-N(1)	2.185(2)
Co(01)-O(3)	2.127(2)	Co(01)-N(1)#1	2.185(2)

Symmetry transformations used to generate equivalent atoms: #1 -x+5/4,-y+5/4,z

Table S2: Selected bond angles observed in [Co(bpds)(bdc)(H_2O)$_2$].bpds, **1**.

Angle	Amplitude (º)	Angle	Amplitude (º)
O(1)-Co(01)-O(1)#1	175.04(12)	O(3)-Co(01)-N(1)	177.88(10)
O(1)-Co(01)-O(3)	90.23(9)	O(3)#1-Co(01)-N(1)	86.76(10)
O(1)#1-Co(01)-O(3)	86.29(9)	O(1)-Co(01)-N(1)#1	94.01(9)
O(1)-Co(01)-O(3)#1	86.30(9)	O(1)#1-Co(01)-N(1)#1	89.33(8)
O(1)#1-Co(01)-O(3)#1	90.23(9)	O(3)-Co(01)-N(1)#1	86.76(10)
O(3)-Co(01)-O(3)#1	91.15(15)	O(3)#1-Co(01)-N(1)#1	177.88(10)
O(1)-Co(01)-N(1)	89.33(8)	N(1)-Co(01)-N(1)#1	95.34(13)
O(1)#1-Co(01)-N(1)	94.02(9)		

Symmetry transformations used to generate equivalent atoms: #1 -x+5/4,-y+5/4,z

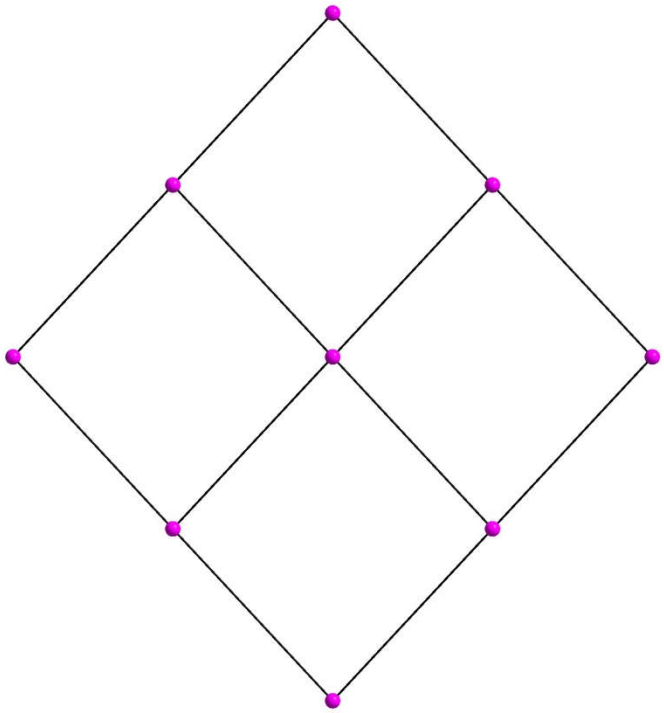

Fig. S6. Figure shows the 4,4-network in [Co(bpds)(bdc)(H_2O)$_2$].bpds, **1**.

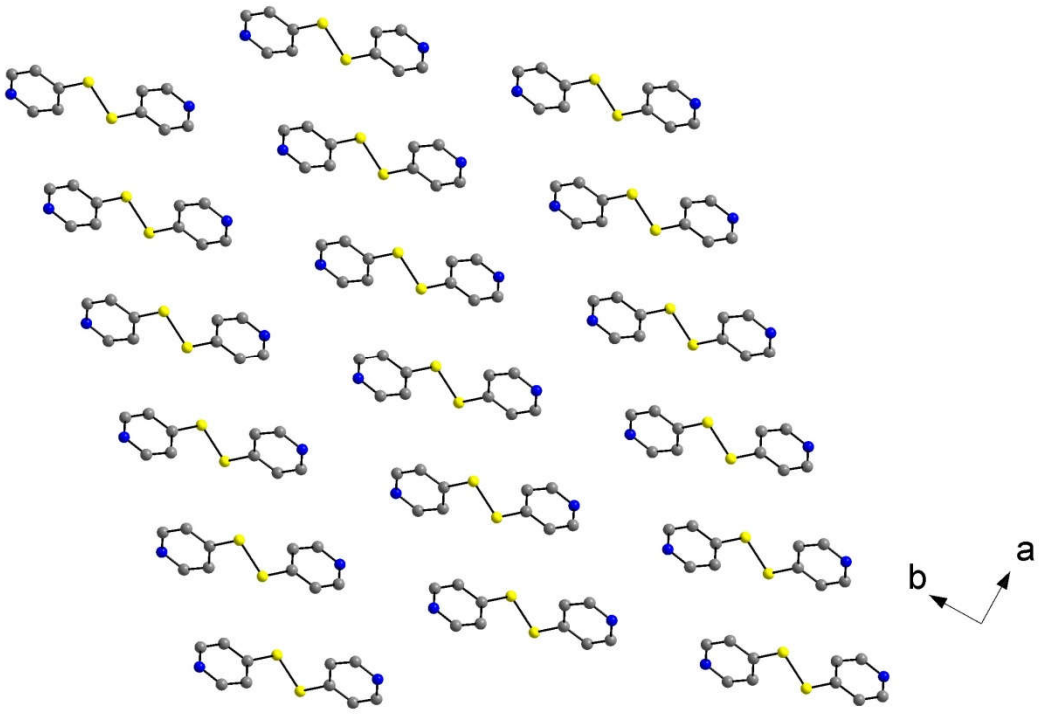

Fig. S7. Figure shows the arrangement of non-bonded bpds in the inter-layer position of $[Co(bpds)(bdc)(H_2O)_2].bpds$, **1**.

Table S3: Potential Hydrogen bonds (Å) observed in [Co(bpds)(bdc)(H_2O)$_2$].bpds, **1**.

Donor --- H....Acceptor	D - H, Å	H...A, Å	D...A, Å	D - H...A, Degree
O(3)--H(3A)..N(2)$^{\#1}$	0.77	2.11	2.8694(2)	166
O(3)--H(3B)..O(2)^{Intra}	0.82	1.92	2.6875(2)	157

Symmetry operations used to generate equivalent atoms: #1 1-x,1/4+y,1/4+z

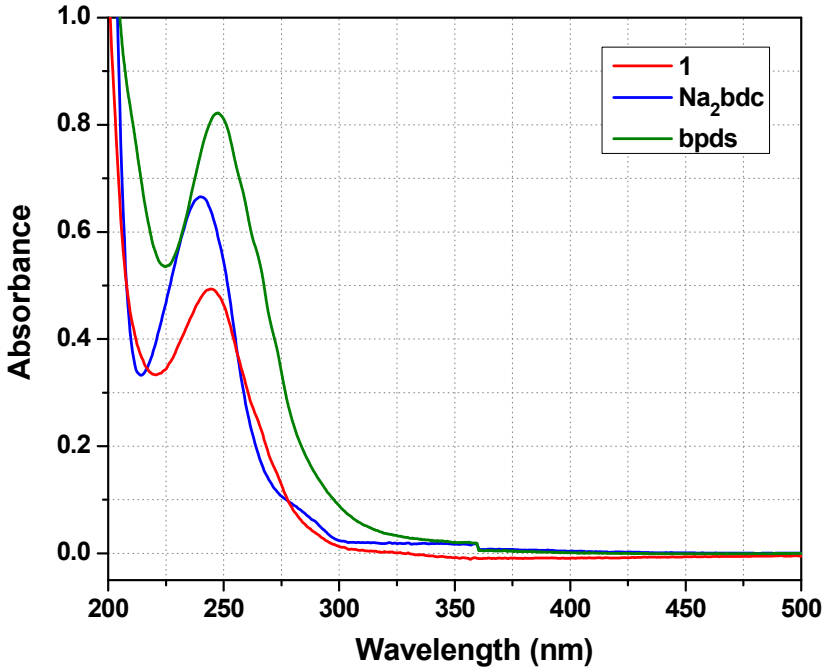

Fig. S8. UV-visible absorption spectra of **1** and the ligands (bpds and Na_2bdc).

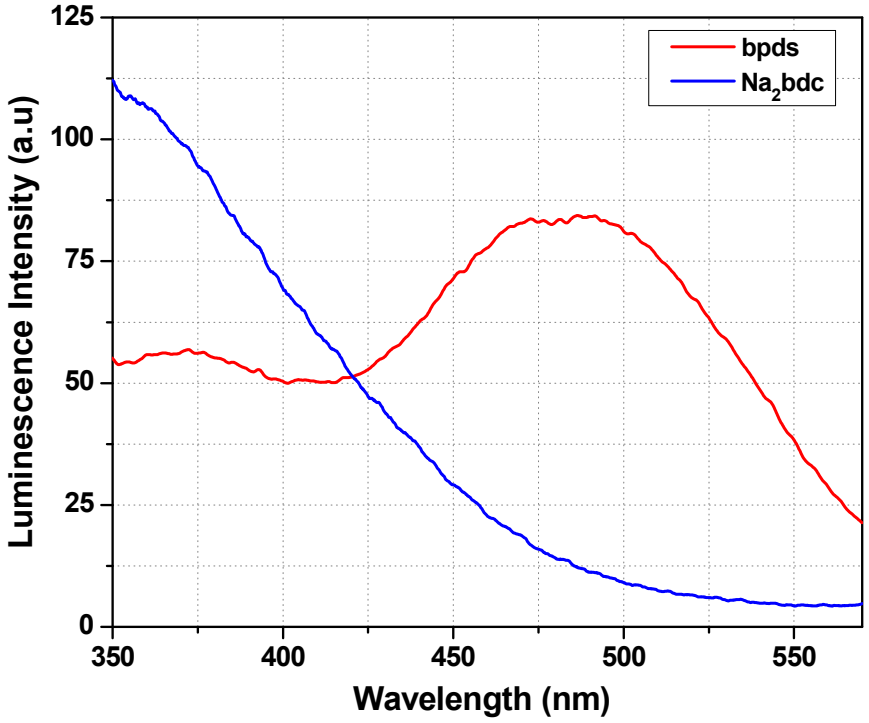

Fig. S9. Emission spectra of bpds and Na_2bdc excited at 300 nm.

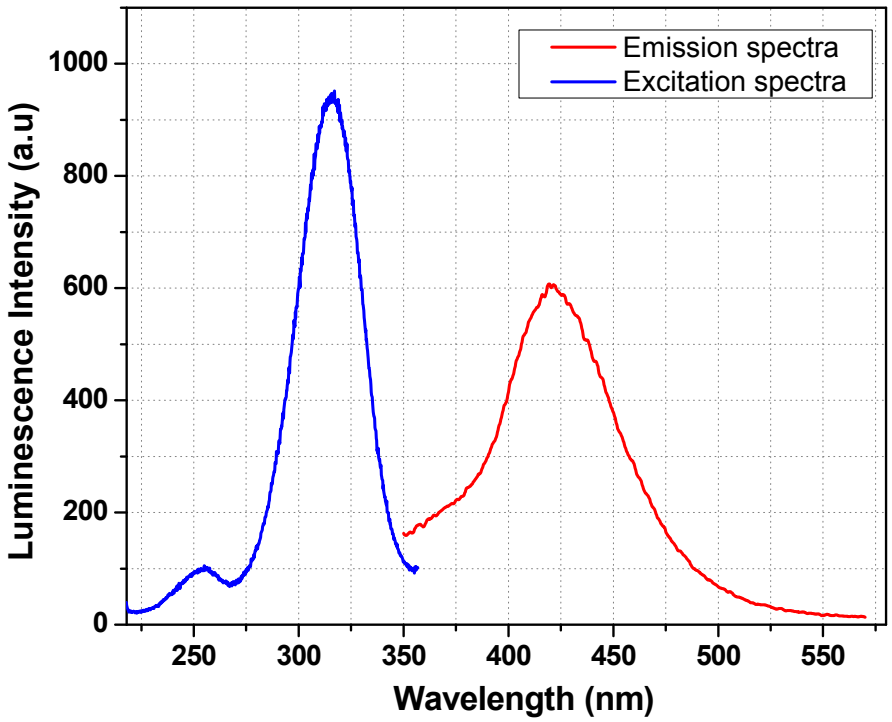

Fig. S10. Excitation and emission spectra of **1**. The excitation wavelength was chosen at 300 nm for emission spectra and for the excitation spectra, emission was fixed at 421 nm.

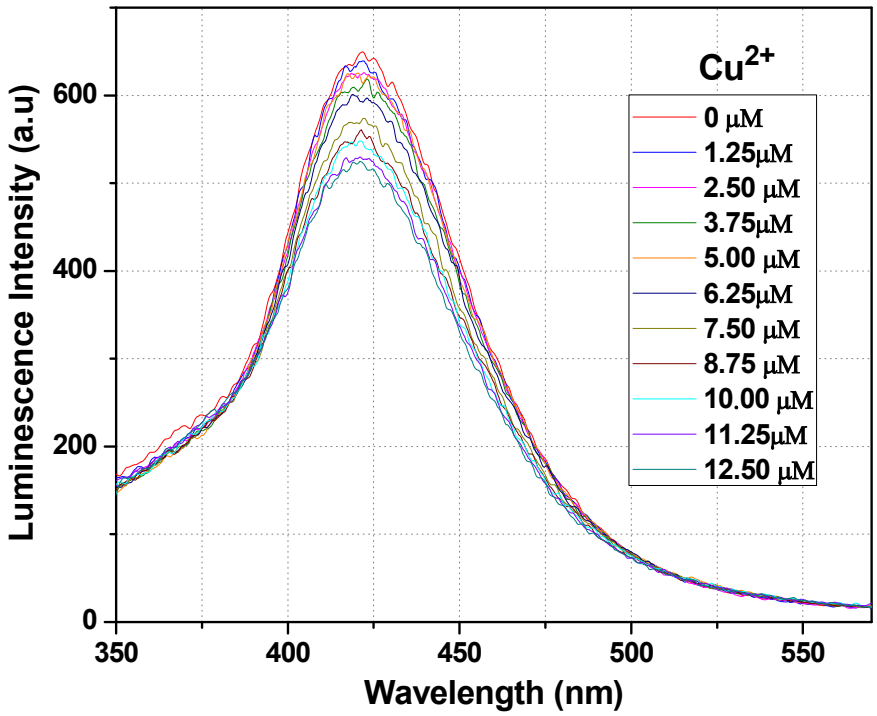

Fig. S11. Emission spectra of **1** dispersed in water upon incremental addition of Cu^{2+} solution (λ_{ex} = 300 nm). Final concentration of Cu^{2+} in the medium is indicated in the legend.

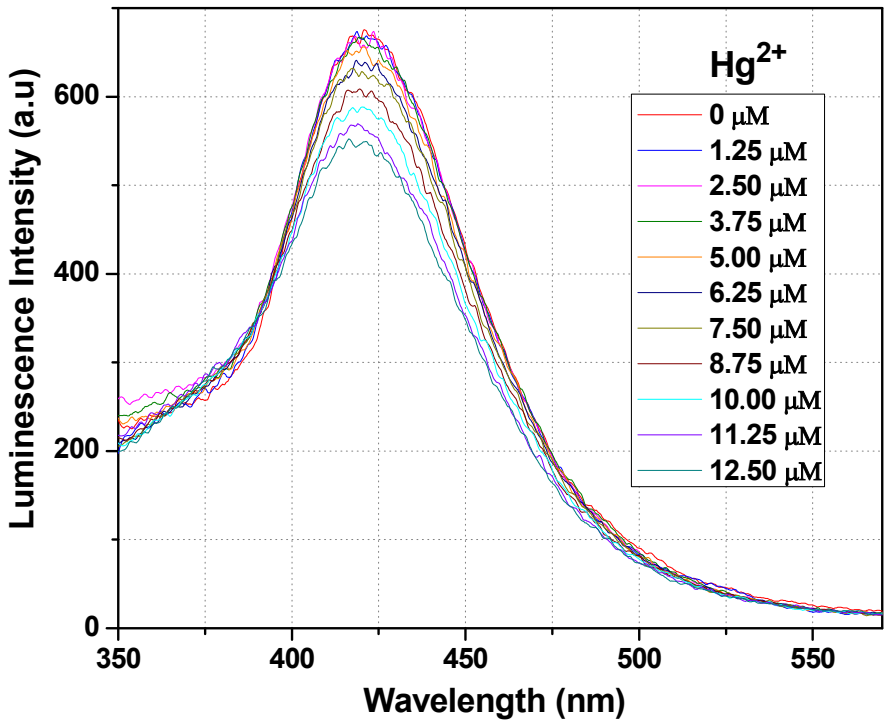

Fig. S12. Emission spectra of **1** dispersed in water upon incremental addition of Hg^{2+} solution (λ_{ex} = 300 nm). Final concentration of Hg^{2+} in the medium is indicated in the legend.

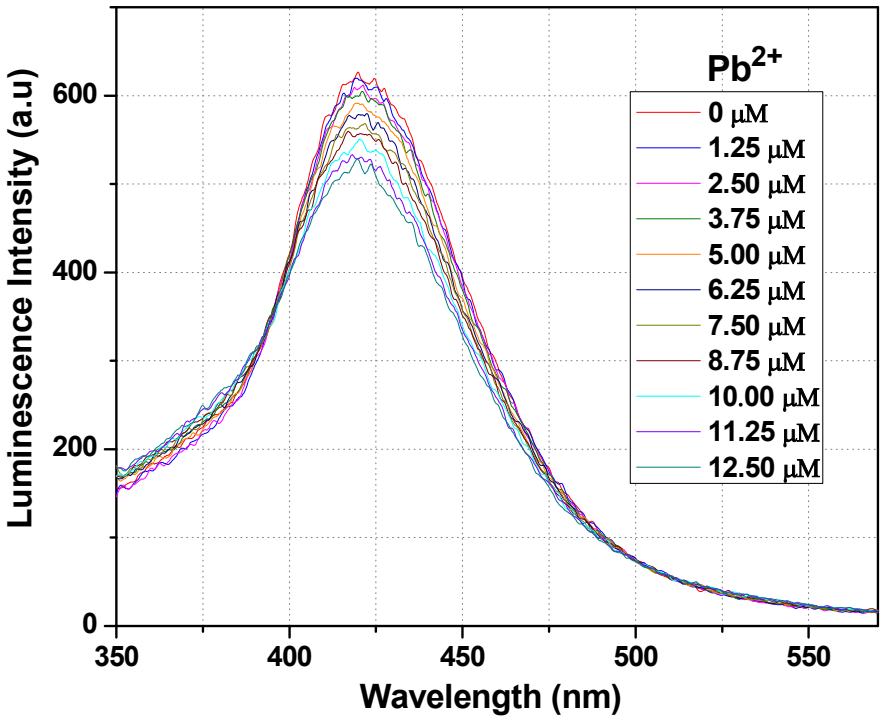

Fig. S13. Emission spectra of **1** dispersed in water upon incremental addition of Pb^{2+} solution (λ_{ex} = 300 nm). Final concentration of Pb^{2+} in the medium is indicated in the legend.

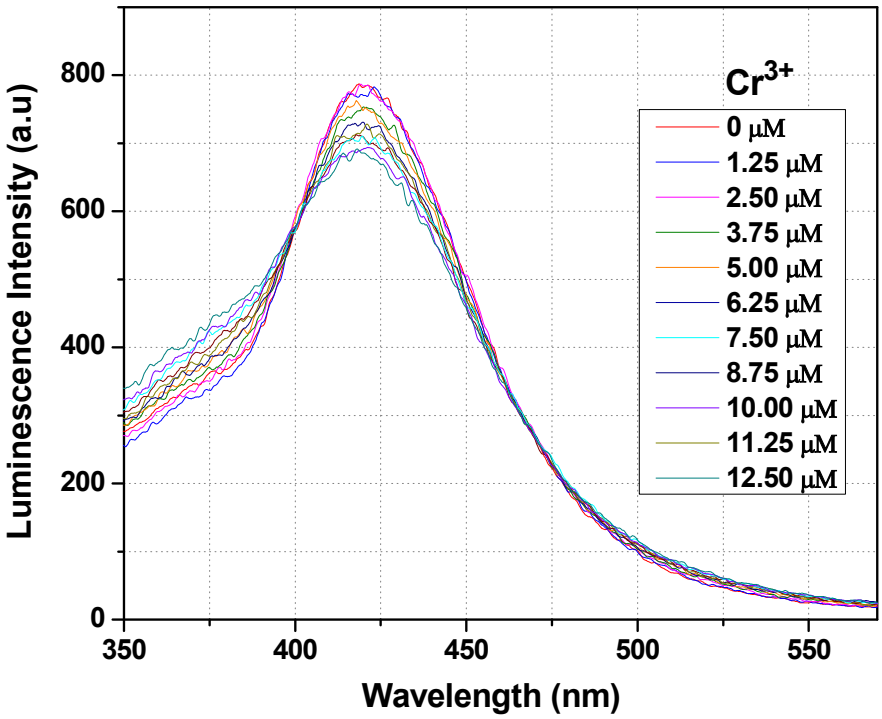

Fig. S14. Emission spectra of **1** dispersed in water upon incremental addition of Cr^{3+} solution (λ_{ex} = 300 nm). Final concentration of Cr^{3+} in the medium is indicated in the legend.

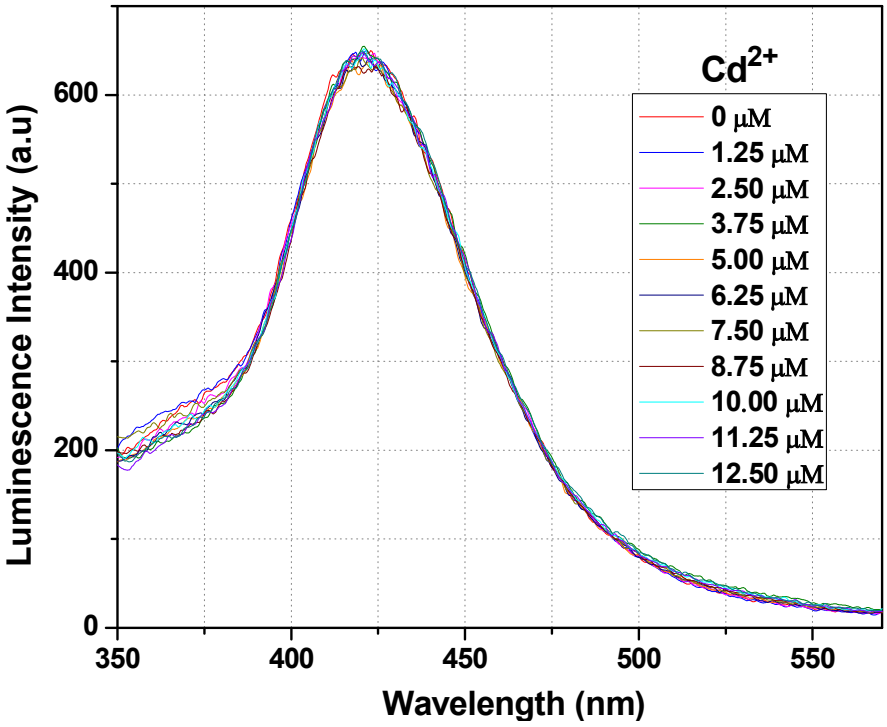

Fig. S15. Emission spectra of **1** dispersed in water upon incremental addition of Cd^{2+} solution (λ_{ex} = 300 nm). Final concentration of Cd^{2+} in the medium is indicated in the legend.

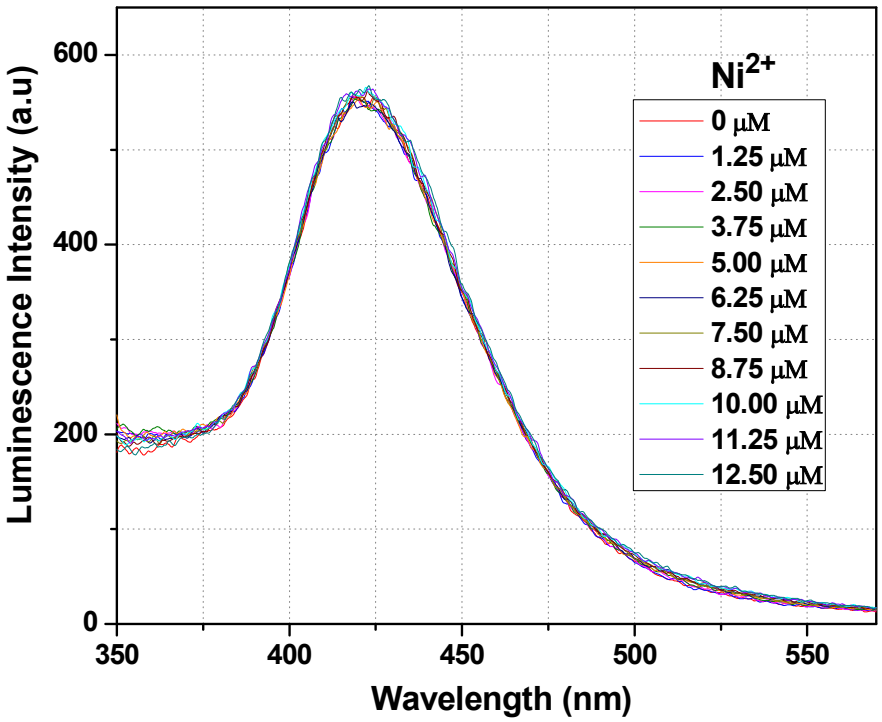

Fig. S16. Emission spectra of **1** dispersed in water upon incremental addition of Ni^{2+} solution (λ_{ex} = 300 nm). Final concentration of Ni^{2+} in the medium is indicated in the legend.

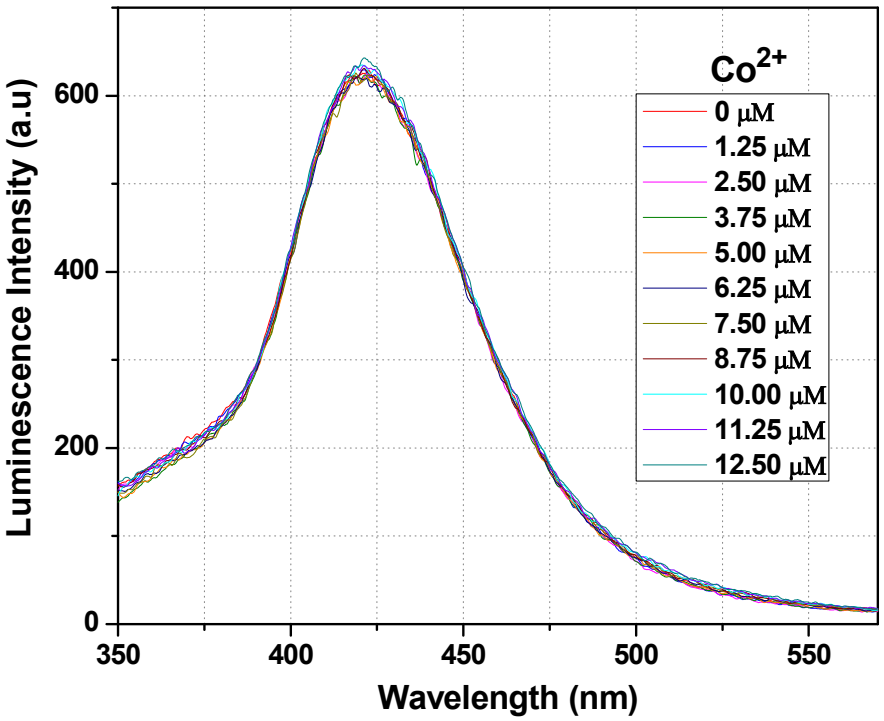

Fig. S17. Emission spectra of **1** dispersed in water upon incremental addition of Co^{2+} solution (λ_{ex} = 300 nm). Final concentration of Co^{2+} in the medium is indicated in the legend.

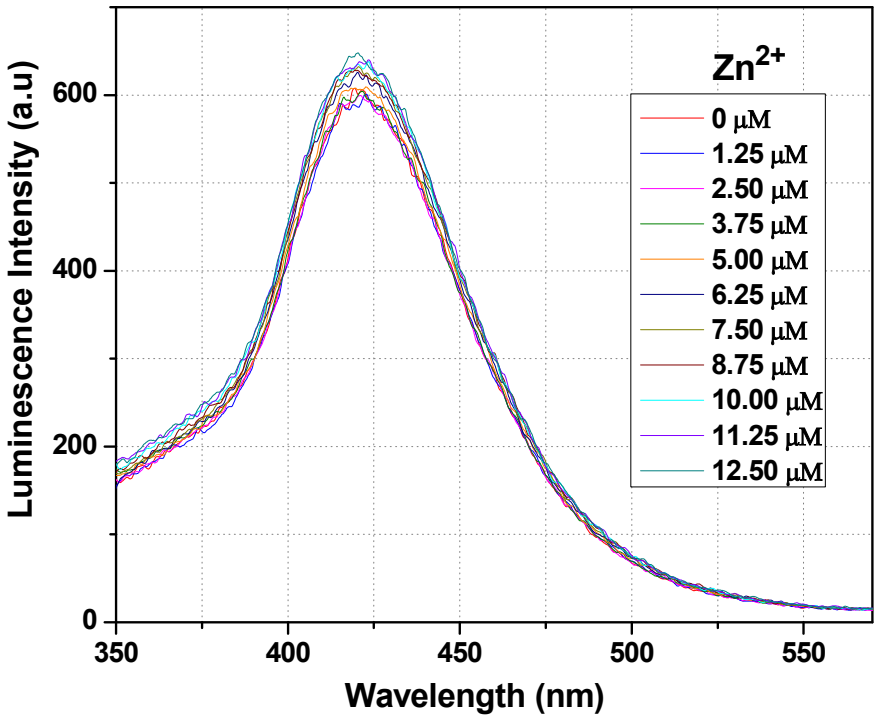

Fig. S18. Emission spectra of **1** dispersed in water upon incremental addition of Zn^{2+} solution (λ_{ex} = 300 nm). Final concentration of Zn^{2+} in the medium is indicated in the legend.

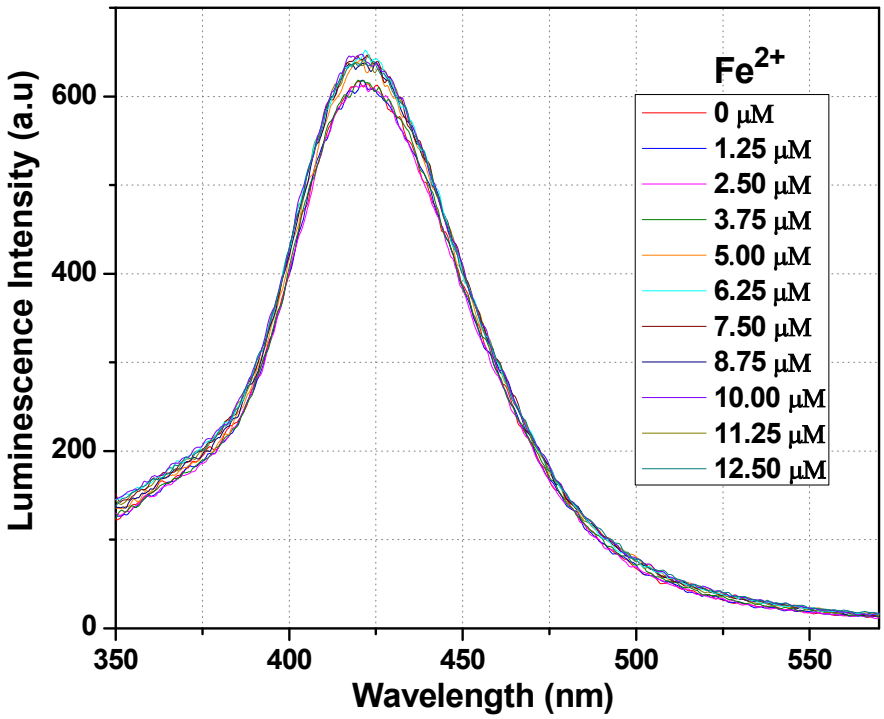

Fig. S19. Emission spectra of **1** dispersed in water upon incremental addition of Fe^{2+} solution (λ_{ex} = 300 nm). Final concentration of Fe^{2+} in the medium is indicated in the legend.

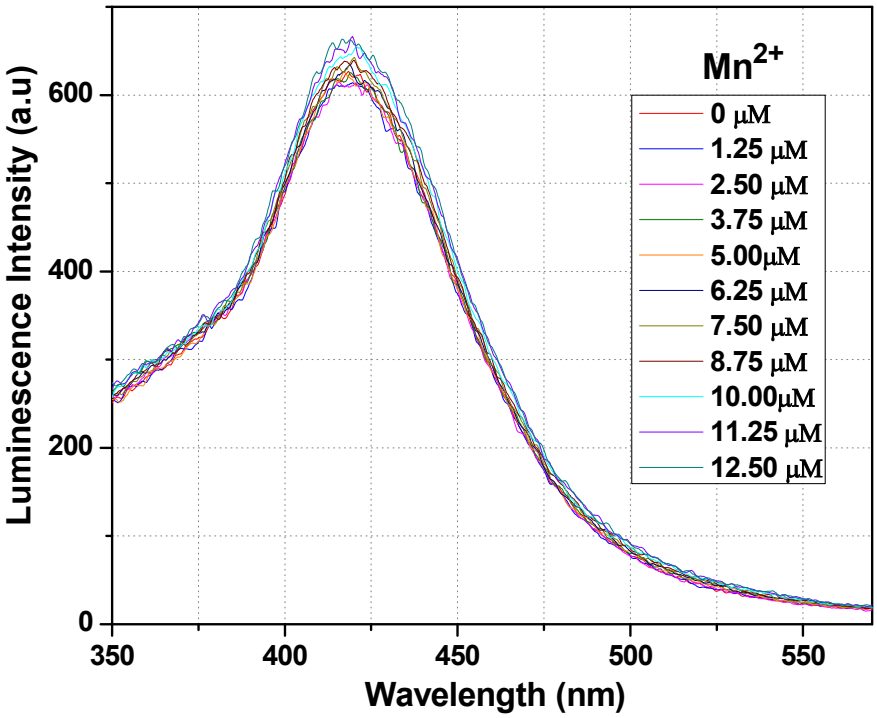

Fig. S20. Emission spectra of **1** dispersed in water upon incremental addition of Mn^{2+} solution (λ_{ex} = 300 nm). Final concentration of Mn^{2+} in the medium is indicated in the legend.

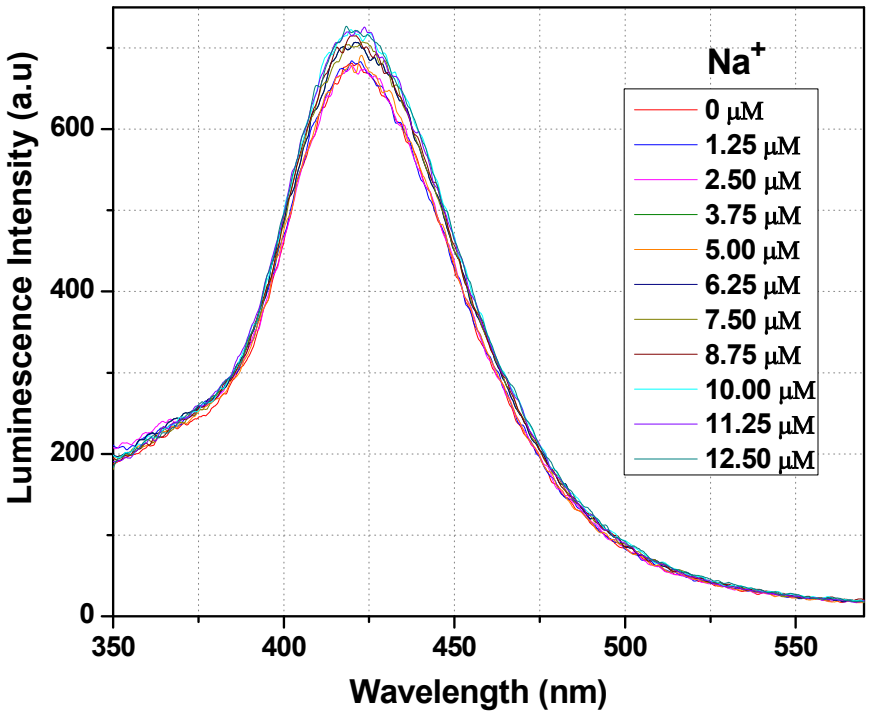

Fig. S21. Emission spectra of **1** dispersed in water upon incremental addition of Na^+ solution (λ_{ex} = 300 nm). Final concentration of Na^+ in the medium is indicated in the legend.

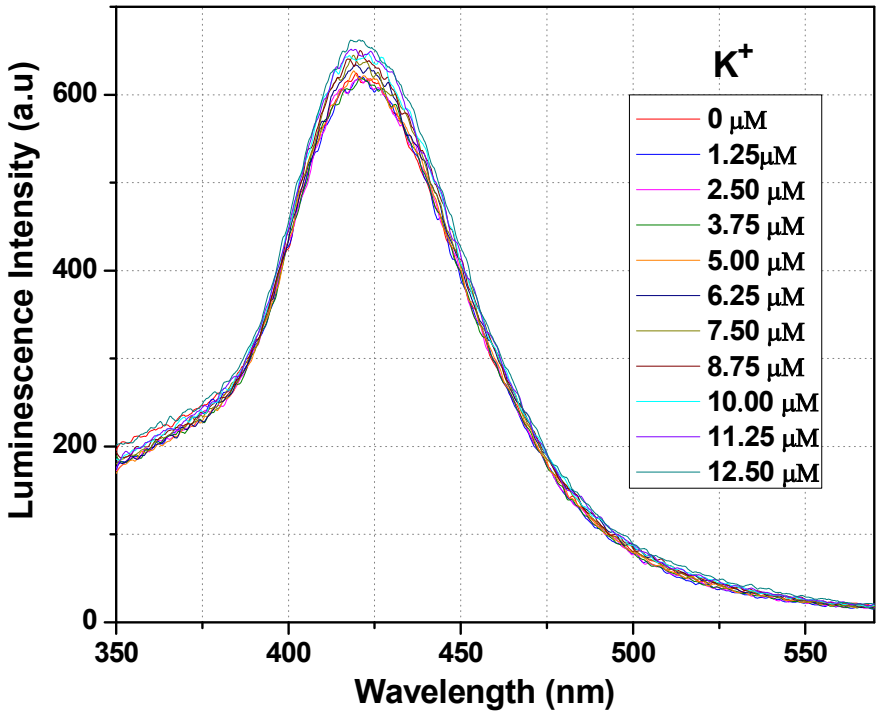

Fig. S22. Emission spectra of **1** dispersed in water upon incremental addition of K^+ solution (λ_{ex} = 300 nm). Final concentration of K^+ in the medium is indicated in the legend.

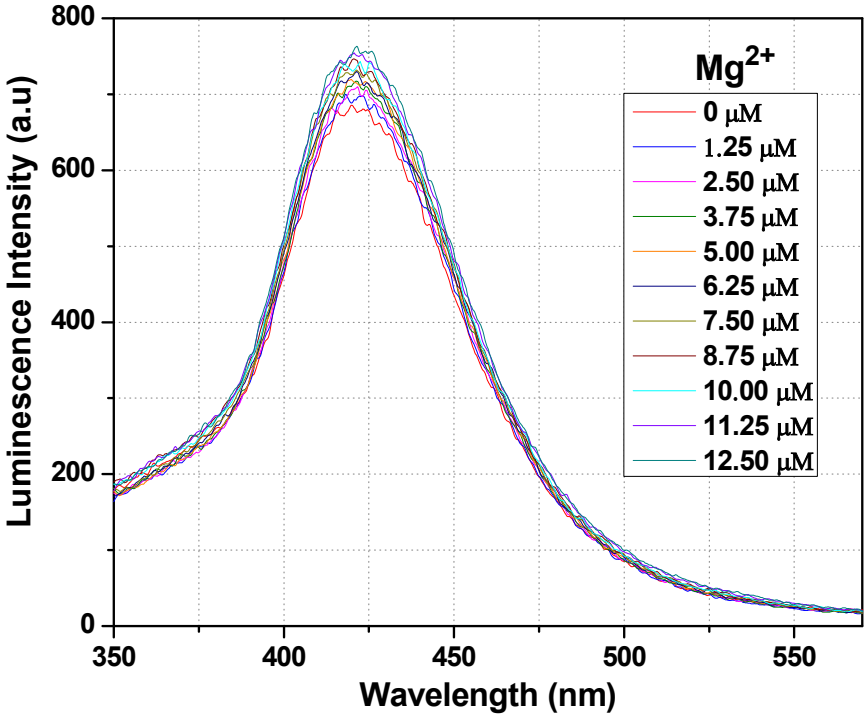

Fig. S23. Emission spectra of **1** dispersed in water upon incremental addition of Mg^{2+} solution (λ_{ex} = 300 nm). Final concentration of Mg^{2+} in the medium is indicated in the legend.

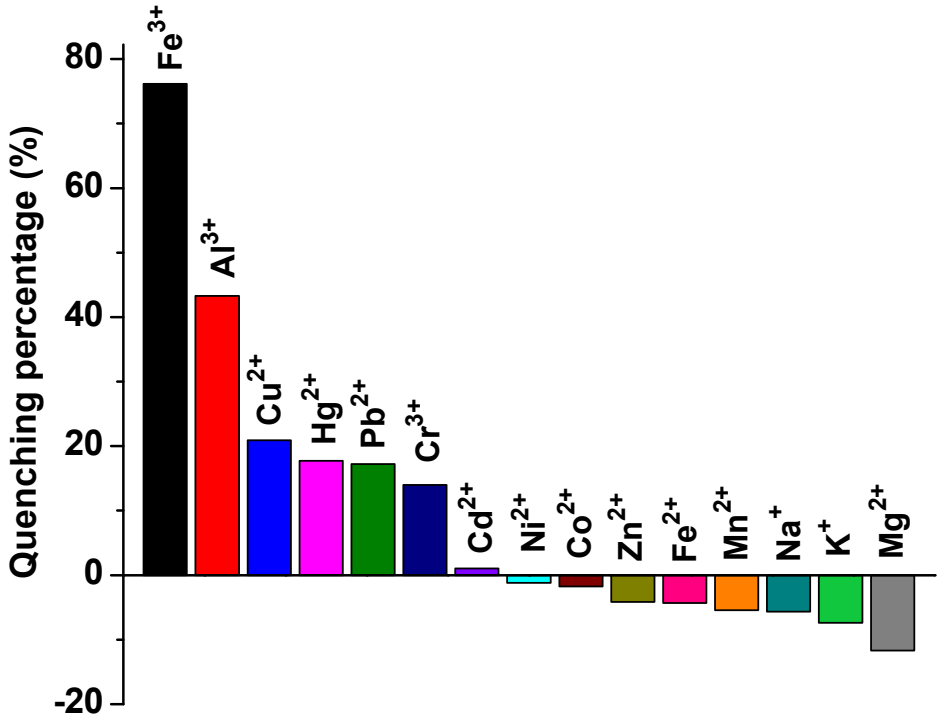

Fig. S24. Change in quenching percentage based on the emission of **1** (at 421 nm) with 12.5 μM of different metal ions. The colour bars are the data points for **1** in presence of the indicated metal ions.

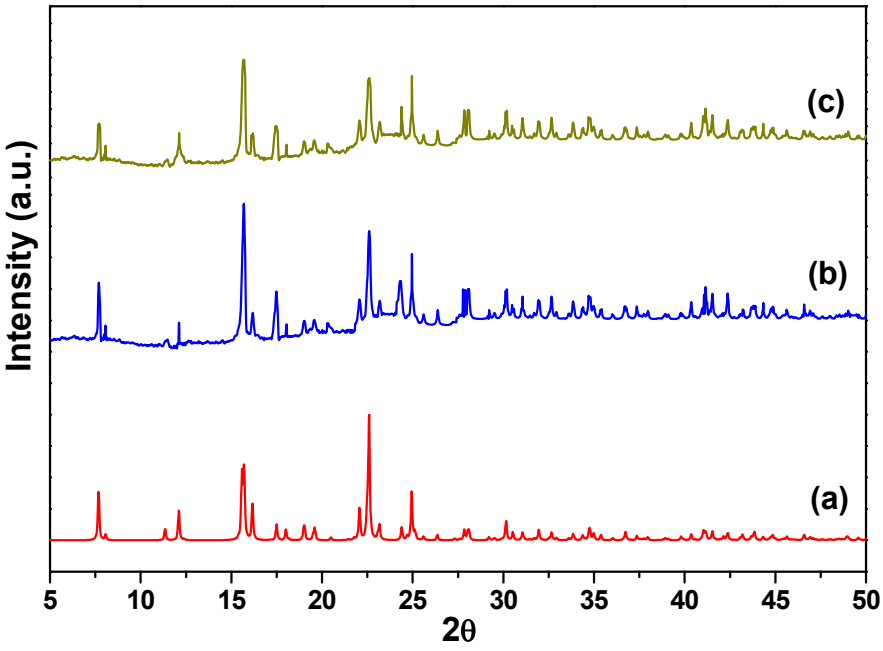

Fig. S25. Powder XRD patterns of **1**, (a) simulated from single crystal X-ray data, (b) after immersing in aqueous solution of Al^{3+} ions and (c) after immersing in aqueous solution of Fe^{3+} ions.

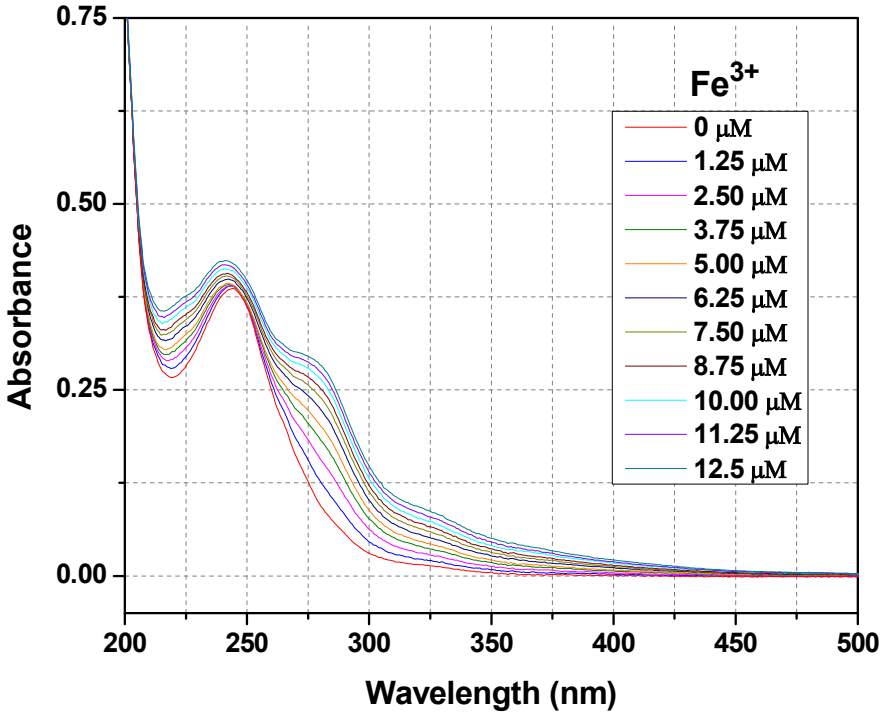

Fig. S26. Absorption spectra of **1** dispersed in water upon incremental addition of Fe^{3+} solution. Final concentration of Fe^{3+} in the medium is indicated in the legend.

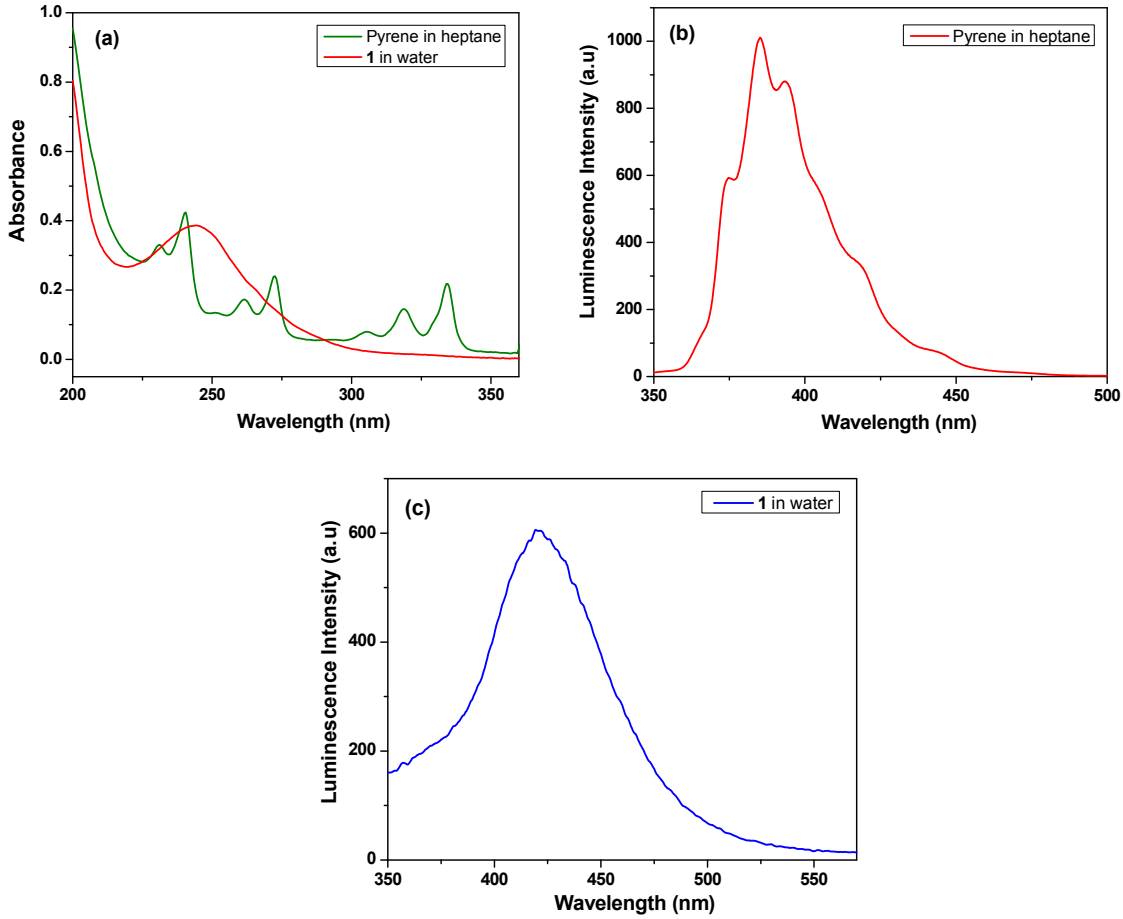

Fig. S27. (a) Absorption spectra of **1** dispersed in water and pyrene in heptane (b) luminescence spectra of pyrene in heptane upon excitation at 300 nm (c) luminescence spectra of **1** dispersed in water upon excitation at 300 nm.

Determination of quantum yield:

$$\boldsymbol{\phi}_f^i = \frac{F^i\, f_s\, n_i^2}{F^s\, f_i\, n_s^2}\, \boldsymbol{\phi}_f^s$$

where $\boldsymbol{\phi}_f^i$ and $\boldsymbol{\phi}_f^s$ are the fluorescence QYs of the sample and that of the standard, respectively; F^i and F^s are the integrated intensities (areas) of sample and standard spectra, respectively; $f_s$and f_i are the absorbance factor of standard and sample, respectively; the refractive indices of the sample and reference solution are n_i and n_s, respectively.

$$\boldsymbol{\phi}_f^i = \frac{49453 \times 0.0365 \times 1.33^2}{51744 \times\ 0.0304 \times 1.38^2} \times\ 0.3$$

$$\boldsymbol{\phi}_f^i = \mathbf{0.32}$$

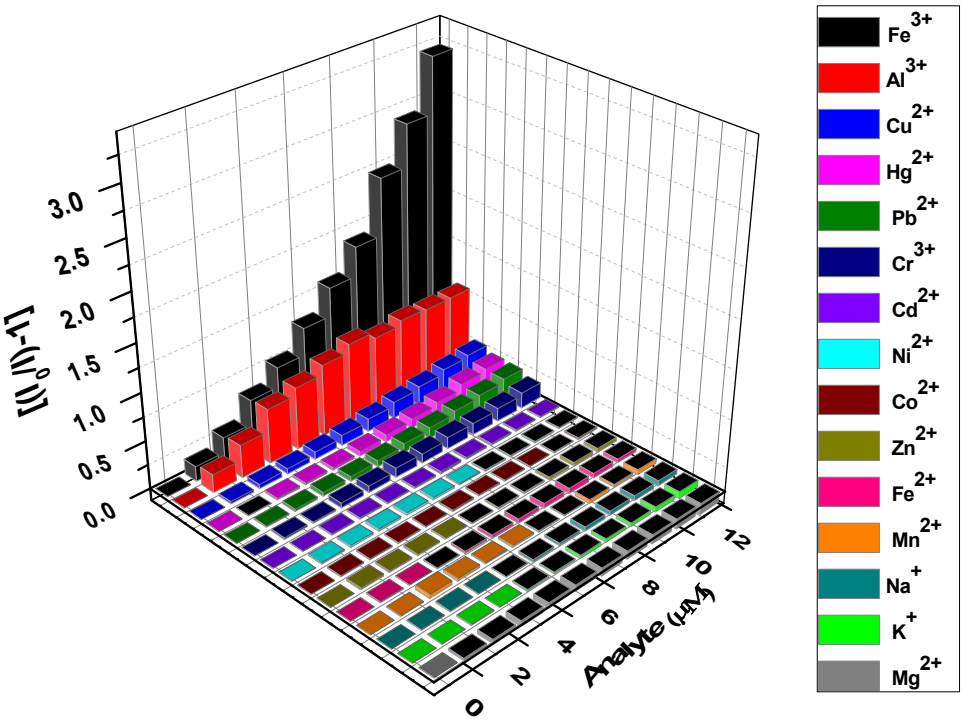

Fig. S28. Plot of $[(I_0/I)-1)]$ of **1** *vs.* concentration of analytes having concentration range of analytes up to 12.5 μM.

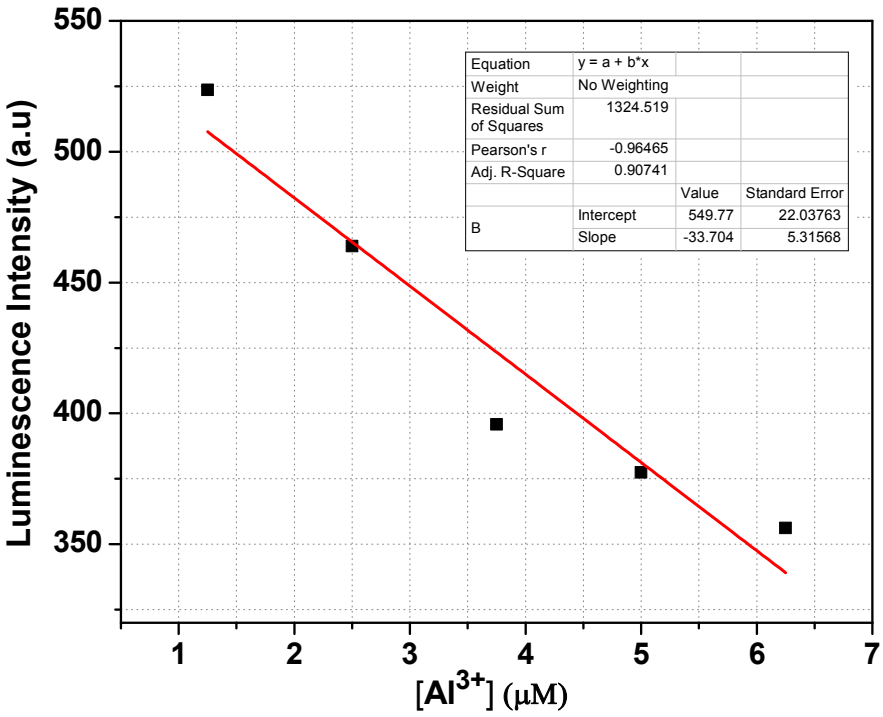

Fig. S29. Change in the Luminescence intensity of **1** in aqueous solution as a function of Al^{3+} concentration.

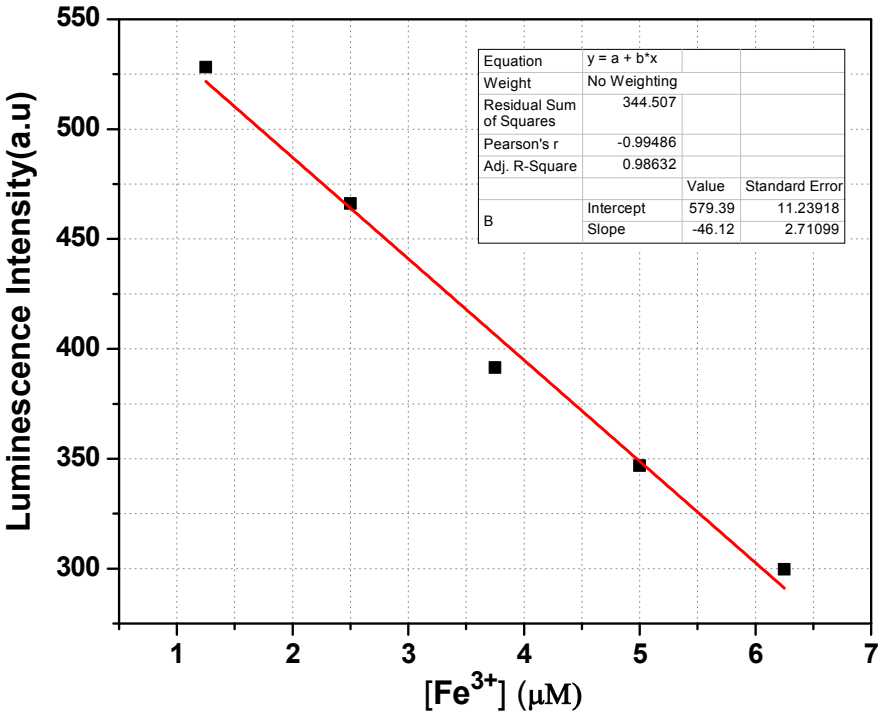

Fig. S30. Change in the Luminescence intensity of **1** in aqueous solution as a function of Fe^{3+} concentration.

Table S4: Calculation of standard deviation and Limit of Detection (LOD) for Al^{3+} and Fe^{3+}:

Blank Reading (only **1**)	Fluorescence Intensities at 421 nm (X)	Mean (x)	Standard Deviation (σ) = $\sqrt{\frac{\sum \lvert X-x \rvert^2}{N}}$
Reading 1	635.2	638.38	3.954
Reading 2	638.8		
Reading 3	636.1		
Reading 4	635.9		
Reading 5	645.9		

Slope, m for Al^{3+} = 33.70

Slope, m for Fe^{3+} = 46.12

LOD for Al^{3+} = $3\sigma/m$ = (3 × 3.954)/33.70 = 0.35 μM = 8.44 ppb

LOD for Fe^{3+} = $3\sigma/m$ = (3 × 3.954)/46.12 = 0.25 μM = 13.59 ppb

where, σ is the standard deviation and m is the slope of the plot of Luminescence Intensity *vs.* Concentration of analyte.

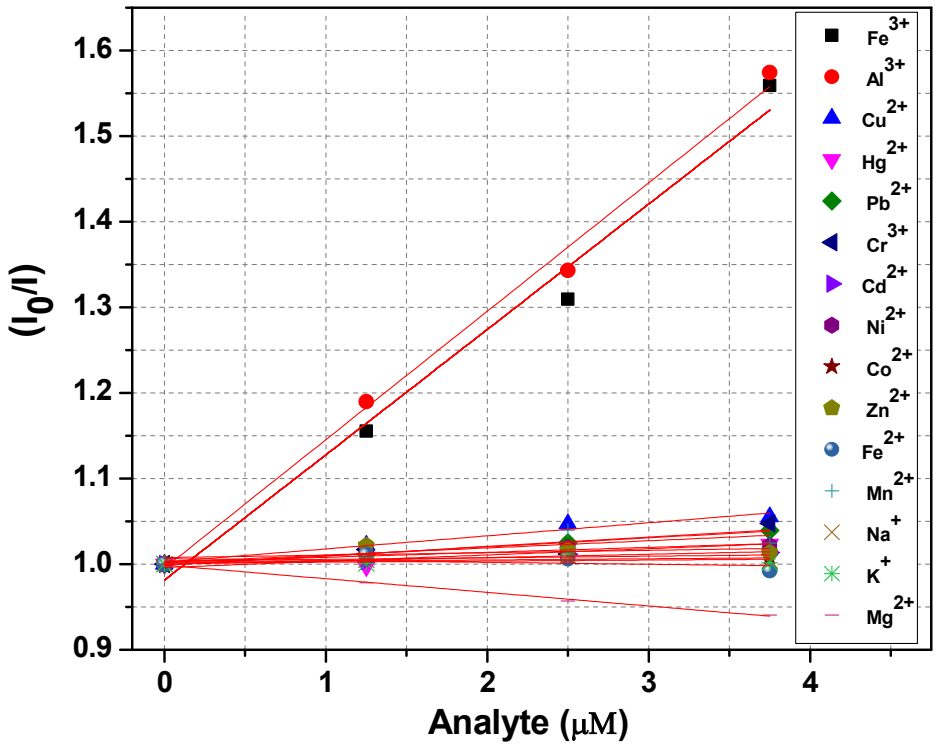

Fig. S31. Plot of luminescence intensity ratio of **1** *vs.* concentration of analytes. I_0 and I are luminescence intensity in absence and presence of analytes, respectively. The slopes indicate the K_{SV} value. The red lines are the best fitted lines to the experimental data.

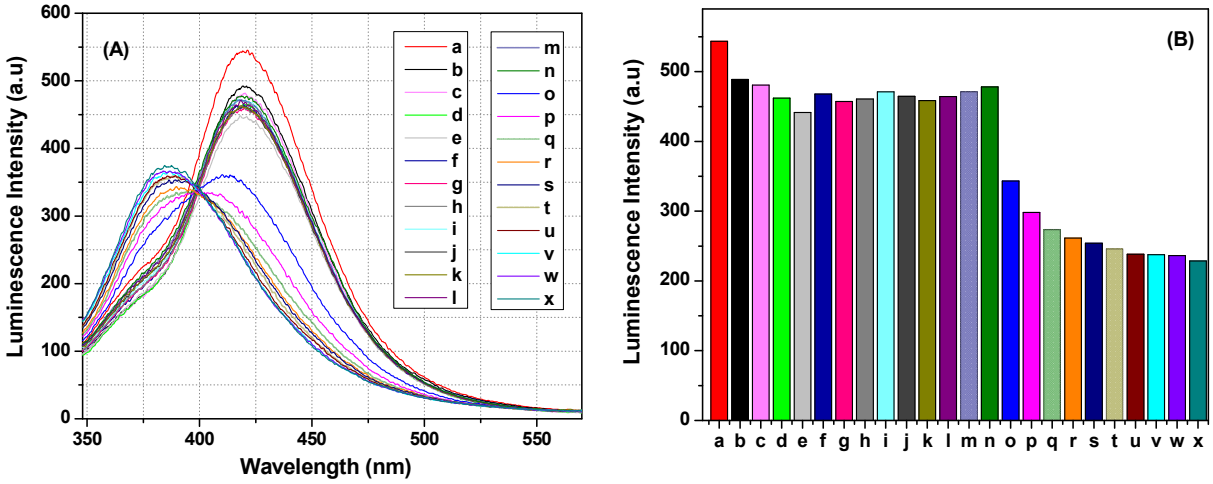

Fig. S32. (A) Emission spectra of **1** dispersed in aqueous solution upon the sequential addition of different metal ions followed by Al^{3+} solution (λ_{ex} = 300 nm). (B) Bar diagram showing the luminescence intensity (monitored at 421 nm) after the sequential addition of other metal ions and Al^{3+} ion. The composition and concentration of the system were as follows: (a) **1** in aqueous solution, (b) a + 2.5 μM Cu^{2+}, (c) b + 2.5 μM Hg^{2+}, (d) c + 2.5 μM Pb^{2+}, (e) d + 2.5 μM Cr^{3+}, (f) e + 2.5 μM Cd^{2+}, (g) f + 2.5 μM Ni^{2+}, (h) g + 2.5 μM Co^{2+}, (i) h + 2.5 μM Zn^{2+}, (j) i + 2.5 μM Fe^{2+}, (k) j + 2.5 μM Mn^{2+}, (l) k + 2.5μM Na^{+} (m) l + 2.5 μM K^{+}, (n) m + 2.5 μM Mg^{2+}, (o) n + 1.25 μM Al^{3+}, (p) n + 2.5 μM Al^{3+}, (q) n + 3.75 μM Al^{3+}, (r) n + 5 μM Al^{3+}, (s) n + 6.25 μM Al^{3+}, (t) n + 7.5 μM Al^{3+}, (u) n + 8.25 μM Al^{3+}, (v) n + 10 μM Al^{3+}, (w) n + 11.25 μM Al^{3+} and (x) n + 12.5 μM Al^{3+}.

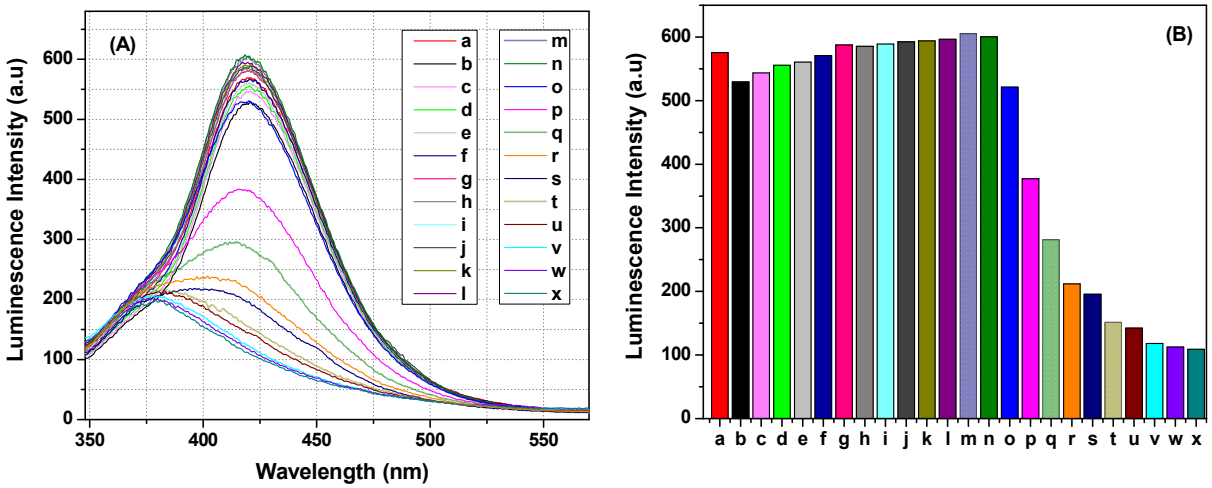

Fig. S33. (A) Emission spectra of **1** dispersed in aqueous solution upon the sequential addition of different metal ions followed by Fe^{3+} solution (λ_{ex} = 300 nm). (B) Bar diagram showing the luminescence intensity (monitored at 421 nm) after the sequential addition of the other metal ions and Fe^{3+} ion. The composition and concentration of the system were as follows: (a) **1** in aqueous solution, (b) a + 2.5 µM Cu^{2+}, (c) b + 2.5 µM Hg^{2+}, (d) c + 2.5 µM Pb^{2+}, (e) d + 2.5 µM Cr^{3+}, (f) e + 2.5 µM Cd^{2+}, (g) f + 2.5 µM Ni^{2+}, (h) g + 2.5 µM Co^{2+}, (i) h + 2.5 µM Zn^{2+}, (j) i + 2.5 µM Fe^{2+}, (k) j + 2.5 µM Mn^{2+}, (l) k + 2.5µM Na^{+} (m) l + 2.5 µM K^{+}, (n) m + 2.5 µM Mg^{2+}, (o) n + 1.25 µM Fe^{3+}, (p) n + 2.5 µM Fe^{3+}, (q) n + 3.75 µM Fe^{3+}, (r) n + 5 µM Fe^{3+}, (s) n + 6.25 µM Fe^{3+}, (t) n + 7.5 µM Fe^{3+}, (u) n + 8.25 µM Fe^{3+}, (v) n + 10 µM Fe^{3+}, (w) n + 11.25 µM Fe^{3+} and (x) n + 12.5 µM Fe^{3+}.

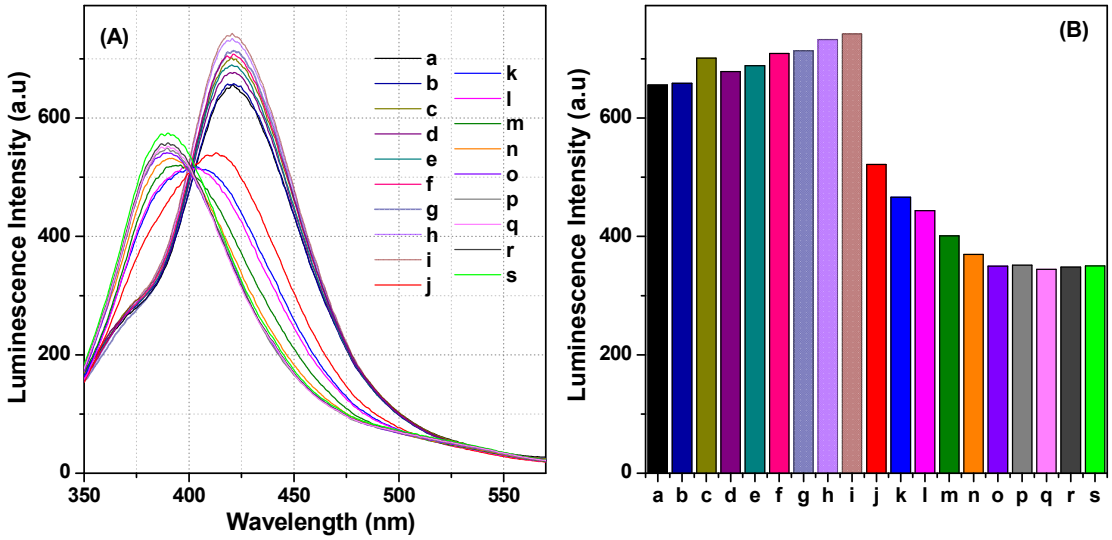

Fig. S34. (A) Emission spectra of **1** dispersed in aqueous solution upon the sequential addition of different anions followed by Al^{3+} solution (λ_{ex} = 300 nm). (B) Bar diagram showing the luminescence intensity (monitored at 421 nm) after the sequential addition of the other anions and Al^{3+} ion. The composition and concentration of the system were as follows: (a) **1** in aqueous solution, (b) a + 2.5 μM Cl^-, (c) b + 2.5 μM F^-, (d) c + 2.5 μM Br^-, (e) d + 2.5 μM I^-, (f) e + 2.5 μM CO_3^{2-}, (g) f + 2.5 μM NO_2^-, (h) g + 2.5 μM NO_3^-, (i) h + 2.5 μM SO_4^{2-}, (j) i + 1.25 μM Al^{3+}, (k) i + 2.5 μM Al^{3+}, (l) i + 3.75 μM Al^{3+} (m) i + 5 μM Al^{3+}, (n) i + 6.25 μM Al^{3+}, (o) i + 7.5 μM Al^{3+}, (p) i + 8.25 μM Al^{3+}, (q) i + 10 μM Al^{3+}, (r) i + 11.25 μM Al^{3+} and (s) i + 12.5 μM Al^{3+}.

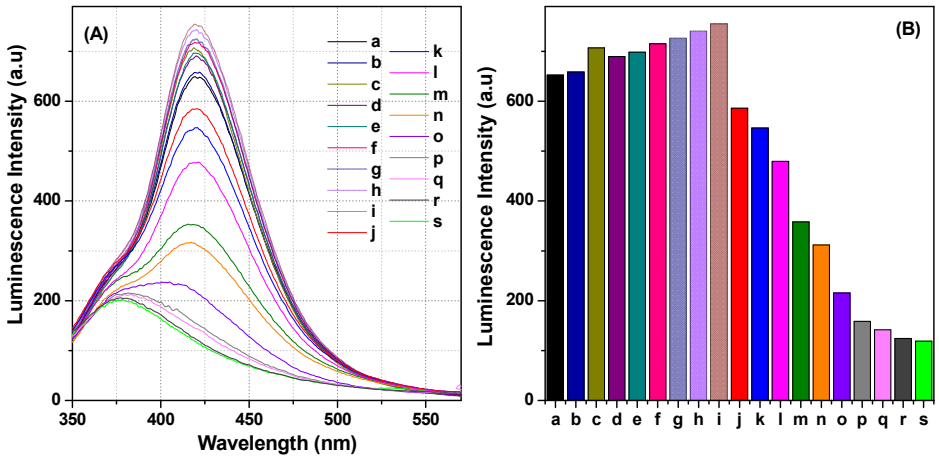

Fig. S35. (A) Emission spectra of **1** dispersed in aqueous solution upon the sequential addition of different anions followed by Fe^{3+} solution (λ_{ex} = 300 nm). (B) Bar diagram showing the luminescence intensity (monitored at 421 nm) after the sequential addition of the other anions and Fe^{3+} ion. The composition and concentration of the system were as follows: (a) **1** in aqueous solution, (b) a + 2.5 µM Cl^-, (c) b + 2.5 µM F^-, (d) c + 2.5 µM Br^-, (e) d + 2.5 µM I^-, (f) e + 2.5 µM CO_3^{2-}, (g) f + 2.5 µM NO_2^-, (h) g + 2.5 µM NO_3^-, (i) h + 2.5 µM SO_4^{2-}, (j) i + 1.25 µM Fe^{3+}, (k) i + 2.5 µM Fe^{3+}, (l) i + 3.75 µM Fe^{3+}, (m) i + 5 µM Fe^{3+}, (n) i + 6.25 µM Fe^{3+}, (o) i + 7.5 µM Fe^{3+}, (p) i + 8.25 µM Fe^{3+}, (q) i + 10 µM Fe^{3+}, (r) i + 11.25 µM Fe^{3+} and (s) i + 12.5 µM Fe^{3+}.

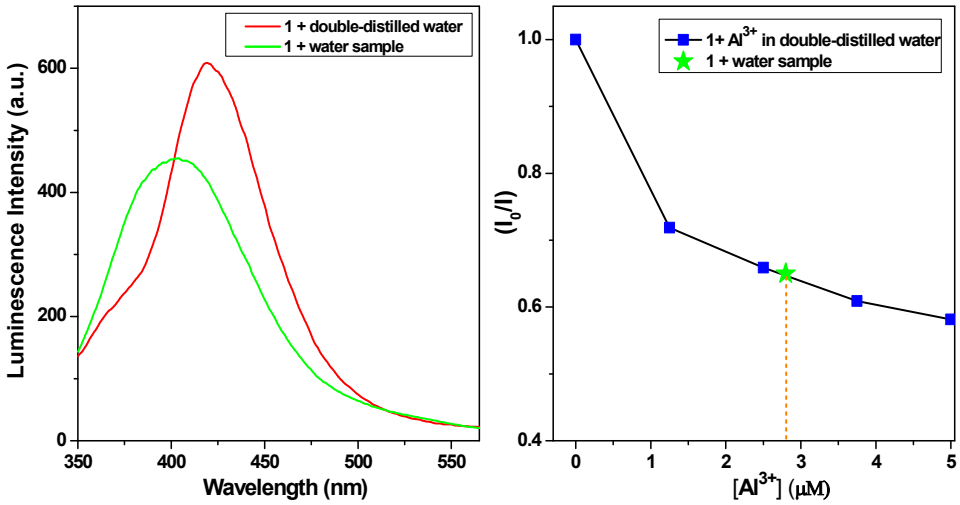

Fig. S36. (A) The emission spectra of **1** in double-distilled water and in water sample. (B) Stern-Volmer plot of luminescence intensity ratio (I_0/I) of **1** monitored at 380 nm *vs* concentration of Al^{3+} ion. I_0 and I represent the luminescence intensity of **1** in absence and presence of Al^{3+} ions, respectively. The green point denotes I_0/I ratio for **1** in water sample. The concentration of Al^{3+} in water sample is determined to be 2.8 μM.

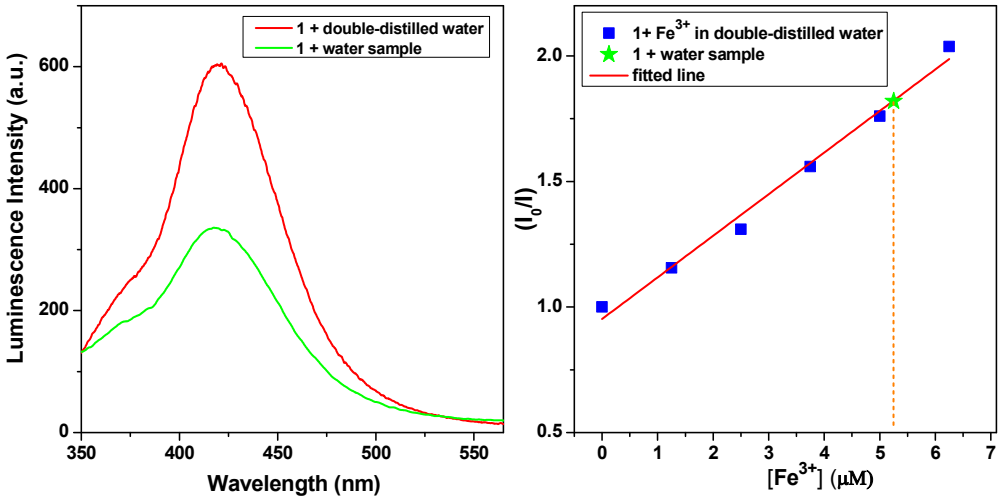

Fig. S37. (A) The emission spectra of **1** in double-distilled water and in water sample. (B) Stern-Volmer plot of luminescence intensity ratio (I_0/I) of **1** monitored at 421 nm *vs* concentration of Fe^{3+} ion. I_0 and I represent the luminescence intensity of **1** in absence and presence of Fe^{3+} ions, respectively. The green point denotes I_0/I ratio for **1** in water sample. The concentration of Fe^{3+} in water sample is determined to be 5.2 μM.